Optics Communications 285 (2012) 5001–5007

Contents lists available at SciVerse ScienceDirect

Optics Communications

journal homepage: www.elsevier.com/locate/optcom

Micro-prism type single-lens 3D aircraft telescope system

Qing-Long Deng [a], Chien-Yue Chen [b,*], Shun-Wen Cheng [b], Wen-Shing Sun [c], Bor-Shyh Lin [d]

[a] Institute of Photonic Systems, National Chiao Tung University, Tainan City 71150, Taiwan
[b] Graduate School of Optoelectronics, National Yunlin University of Science and Technology, Yunlin 64002, Taiwan
[c] Department of Optics and Photonics, National Central University, Taoyuan County 32001, Taiwan
[d] Institute of Imaging and Biomedical Photonics, National Chiao Tung University, Tainan City 71150, Taiwan

ARTICLE INFO

Article history:
Received 20 May 2012
Received in revised form
31 July 2012
Accepted 1 August 2012
Available online 23 August 2012

Keywords:
Three-dimensional image acquisition
Telescopes
Image detection systems
Remote sensing

ABSTRACT

Based on the image payload on an Unmanned Aircraft System, this study utilizes a micro-prism array and single-lens remote camera to assess the feasibility of having two virtual cameras shoot terrain image pairs with inclined $\pm 10^{\circ}$. The software, LightTools, is applied for simulating and verifying the feasibility of the optical system. In comparison with traditional frame-type remote cameras, this study not only could acquire highly overlapped stereoscopic image pairs from different viewing angles, but could also increase the stereoscopic image pairs by two times. The system we propose obtains more stereoscopic digital terrain information than do traditional systems.

1. Introduction

Air-photo remote cameras are commonly utilized to obtain terrain and water images for people's livelihoods and science. Image payloads in airplanes present the function of stereoscopic observation that they could shoot the same terrain image pairs from various angles and produce a digital terrain model from the overlapped area of two-dimensional image pairs [1]. With the miniature electronic system and the mature development of communication technology, Unmanned Aerial Vehicles (UAV), which presents high resolution and added mobility, are applied to the surveys after disasters or for use with steep terrain. Nonetheless, unmanned aircrafts have less load capacity so that only light cameras can be equipped for remote [2].

Three types of remote stereoscopic image pairs are presently classified. With the aircraft moving at a uniform velocity, the first type is the Frame Type vertical photographs with fixed time intervals from which a stereoscopic image pair with a 60% overlapping rate can be acquired from two shots [3]. However, from this type, terrain dead space information is not easily obtained because of the small angle of the view and the vertical imaging. The second type are Three-Line-Scanner (TLS) images with Line Array CCD that images from three directions and can be shot in flight with an included 21° angle and a high overlapping rate [4,5]. Such a method is likely to affect the scanning precision because of jitter that results from flying and thus generates broken and blurred images. The third type is the Inclined Photography Technology with high parallax stereoscopic reproduction which has two or more Digital Single Lens Reflex Cameras (DSLR) horizontally shooting from both ends of the aircraft [6]. With the inclined angle about $\pm 30^{\circ}$ to the image, the stereoscopic image pairs are acquired by front and back positioning. Such a method requires two high-precision remote sensors that can cause a double load problem, increasing cost, consume more power, and require more calibrations for more cameras.

The proposed system is based on a refracting camera [7,8]. Lee et al. equipped a biprism in front of an ordinary camera and acquired one-shot-two-views [9]. This was accomplished by replacing the traditional stereoscopic imaging system with two cameras. Chen et al. proposed imaging technology with a micro-prism type single lens stereoscopic camera in 2008. In comparison with the biprism, a micro-prism allows reducing the volume and the weight of the system as well as improving the chromatic aberration of prisms [10].

In addition to the concept of one-shot-two-views in the micro-prism type single lens stereoscopic photography, a micro-prism array is equipped on the airborne frame type telecamera so that the optical characteristics of prisms could deflect the optical path and allow the vertical imaging system to be inclined to reduce the terrain dead space. Besides, obtaining terrain image pairs with one shot could largely increase the quantity of stereoscopic image pairs. The micro-prisms produced

* Corresponding author. Tel.: +886 5 5342601x4344; fax: +886 5 5312063.
E-mail address: chencyue@yuntech.edu.tw (C.-Y. Chen).

0030-4018/$ - see front matter
http://dx.doi.org/10.1016/j.optcom.2012.08.023

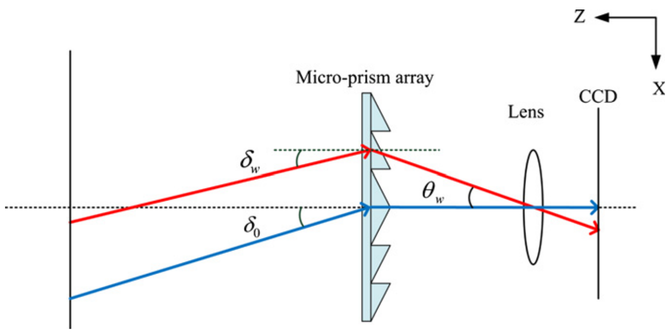

Fig. 1. Deflected field of view through micro-prism array.

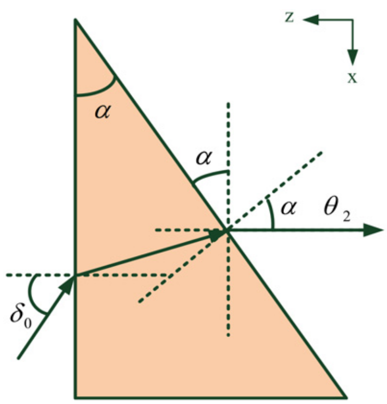

Fig. 2. Relationship between the deflection angle of the FOV and the field of view of half lens.

with micro-optic technology could effectively reduce the volume, the weight, and the cost to improve on the drawbacks of the above airborne imager.

2. Theory

This study designed a stereoscopic terrain imaging system with a micro-prism array equipped on an airborne camera. Fig. 1 shows the symmetrically rectangular prisms in the micro-prism structure so that the lower distribution of FOV of the prism could be theoretically analogized from the upper distribution. Through the micro-prism array, the entire field of view was defined as the deflection angle δ_0 and δ_w, the half angle of the view of lens θ_w, and the incidence of the micro-prism parallel with z-axis. The image width acquired from the half angle of view of the CCD camera could be calculated by δ_0 and δ_w.

The structure of the upper prism was magnified to discuss the relations between the deflection angle of FOV δ_0 and the half angle of the view of lens θ_w, as shown in Fig. 2. First, the clockwise direction included the angle between the light and the normal was defined as positive, and the counterclockwise one as negative. When the incident angle of the light was below the normal being δ_0, the projected light paralleled to z-axis and the included angle between the projected light and the second normal of the micro-prism equaled the vertex angle of the prism α. The equation of δ_0 and the vertex angle α is given by

$$\delta_o = \sin^{-1}\left(\sin\alpha\sqrt{n^2-\sin^2\alpha}-\cos\alpha\sin\alpha\right) \quad (1)$$

In Fig. 3, when the light entered from below the normal to the prism with the incident angle δ_w and the projected light entered

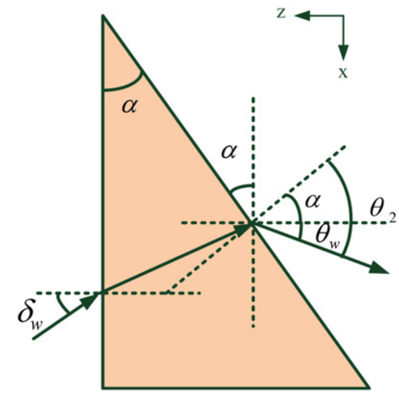

Fig. 3. Relationship between the deflection angle of the FOV and the field of view of half lens.

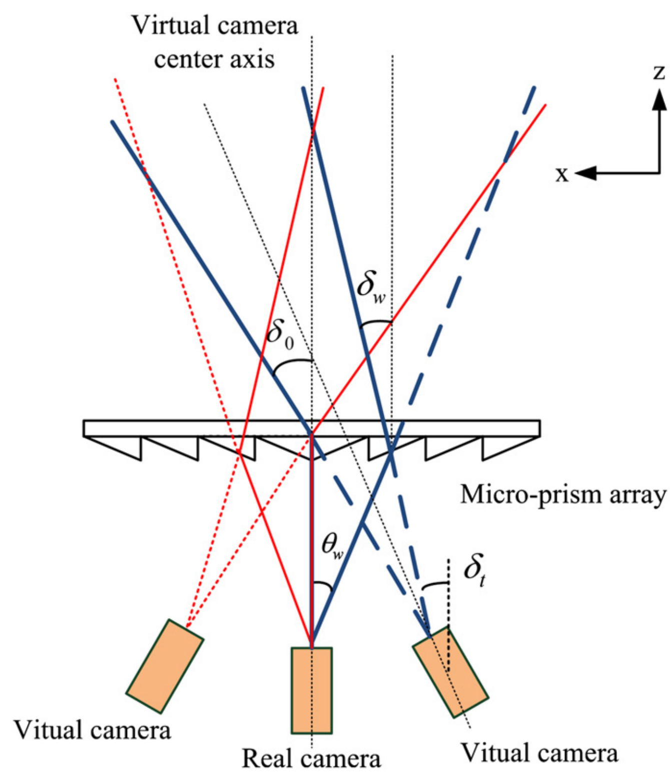

Fig. 4. Imaging with micro-prism array camera.

the half angle of view of the camera θ_w, the projected angle θ_2 equaled the sum of the vertex angle α and the half angle of view θ_w. The equation of δ_w and the half angle of view θ_w is given by

$$\delta_w = \sin^{-1}\left(\sin\alpha\sqrt{n^2-\sin^2(\alpha-\theta_w)}-\cos\alpha\sin(\alpha-\theta_w)\right) \quad (2)$$

When equipping the micro-prism array on the camera, the field of view would deflect with the characteristics of a prism so that the deflected field of view could be defined as the imaged FOV of two virtual cameras, as shown in Fig. 4. The two virtual cameras would incline to the same horizontal position with the left and the right fields of view almost overlapping, but they would separate with the increasing distance to the object. The inclined angle of the optical axis on z-axis of the virtual camera could be defined as δ_t, which could be determined by the

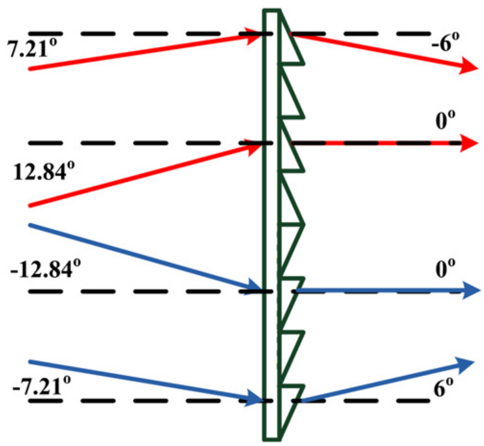

Fig. 5. Horizontal FOV of the prism.

deflection angles of FOV δ_w and δ_0:

$$\delta_t = \frac{\delta_w + \delta_0}{2} \tag{3}$$

2.1. Design

The stereoscopic observation of airborne imagers depends on increasing the inclined angle of imaging to acquire the distanced image pairs with a larger parallax [6]. For this reason, the design refers to a $\pm 10^\circ$ imaging angle of a Three-Line-Scanner (TLS). The inclined angle of optical light of the two virtual cameras δ_t was set at 10° and the deflection angles of FOV δ_w and δ_0 the horizontal angle of view of the camera at 12°. Based on the above requirements of parameters, $\delta_t = 10^\circ$ and the horizontal half angle of view $\theta_w = 6^\circ$ were substituted with Eqs. (1–3) for the optimal deflection angle of FOV δ_w and δ as well as the base angle of prism α. The base angle of the upper micro-prism array α therefore was set at 25.1°. When the incident angle of the light $\delta_0 = 12.84^\circ$, the received optical angle was 0°; and, the received optical angle was -6° when the incident angle $\delta_w = 7.21^\circ$. On the contrary, the base angle of micro-prism array α was -25.1°, the incident angle of micro-prism array $\delta_0 = -12.84^\circ$, and the received optical angle 0°; while the received optical angle was 6° when the incident angle $\delta_w = -7.21^\circ$, as shown in Fig. 5.

2.2. Sampling of stereoscopic image pair

The traditional frame type airborne imagers vertically shot stereoscopic terrain image pairs with the displacement of aircrafts, as shown in Fig. 6(a). Image I_1 was shot at position P_1 and I_2 at P_2 so that I_1 and I_2 could form the stereoscopic image pair with an overlapping rate of 60%. The micro-prism airborne stereoscopic camera imaged the terrain with the inclination method and one-shot-two-views so that it could increase the images by two-fold compared with traditional frame-type cameras, as shown in Fig. 6(b). When the airborne imager shot at position P_1, the image pairs I_{R1} and I_{L1} would be obtained. When the aircraft moved to P_2, another image pair I_{R2} and I_{L2} would also be acquired. By imaging at appropriate timing, I_{L1} and I_{R2} could form a stereoscopic image pair with a more than 95% overlapping rate.

2.3. Design of lens

The optical system was composed of an airborne camera and a micro-prism array (the specifications for the camera sensor are shown in Table 1). In order to correspond to the specifications of the image, the lens aperture was set at f-number = 3 and the effective focal length at $f = 136.7$ mm. Moreover, an aerial camera lens [12] proposed by Laikin was utilized at the primary stage. The obtained imaging quality was further analyzed to assess how well it could meet the design requirements for the specified system. The specifications for the lens are listed in Table 2.

Having the optical software *Zemax* for optimization, the completed lens is shown as Fig. 7(a). The imaging quality was further tested by analyzing the parameters of MTF, curvature, and astigmatism, etc. Fig.7(b) displays the MTF changes of the imaging resolution where tangential rays appeared at the minimum of 45.17% at the field of view 61 lp/mm. Fig. 7(c) presents the relationship between the out-of-focus images and the imaging resolution, where MTF still remained above 30% when the out-of-focus images were between -0.031 mm to 0.043 mm, showing that the imaging quality would decline in quality beyond the range. Fig. 7(d) shows the curvature and the distortion of the

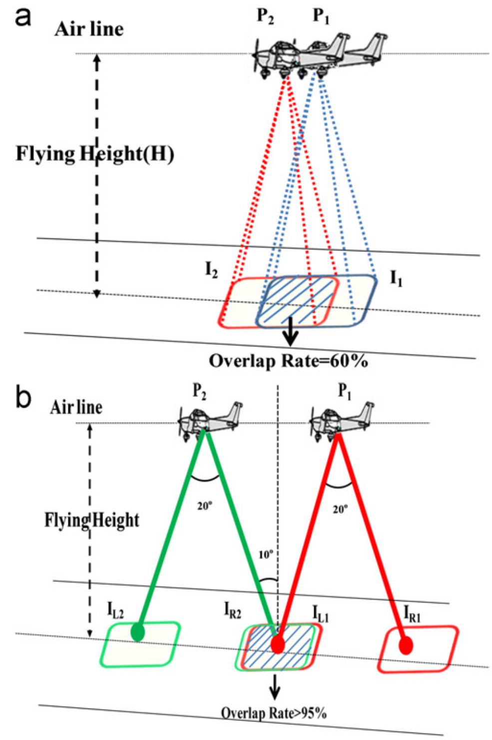

Fig. 6. (a) Imaging with a frame type airborne imager and (b) imaging with a micro-prism airborne stereoscopic camera.

Table 1
Specifications of CCD sensor [11].

Sensor area	3504H × 2336V
Pixel size	8.19 μm × 8.19 μm
H image height (H)	14.35 mm
V image height (V)	9.55 mm
Image area	28.7 mm × 19.1 mm

Table 2
Specifications of lens.

Wavelength range	486nm–656 nm
F number	3
FOV	14.37°
Effective focal length	136.7 mm
θ_w	6°

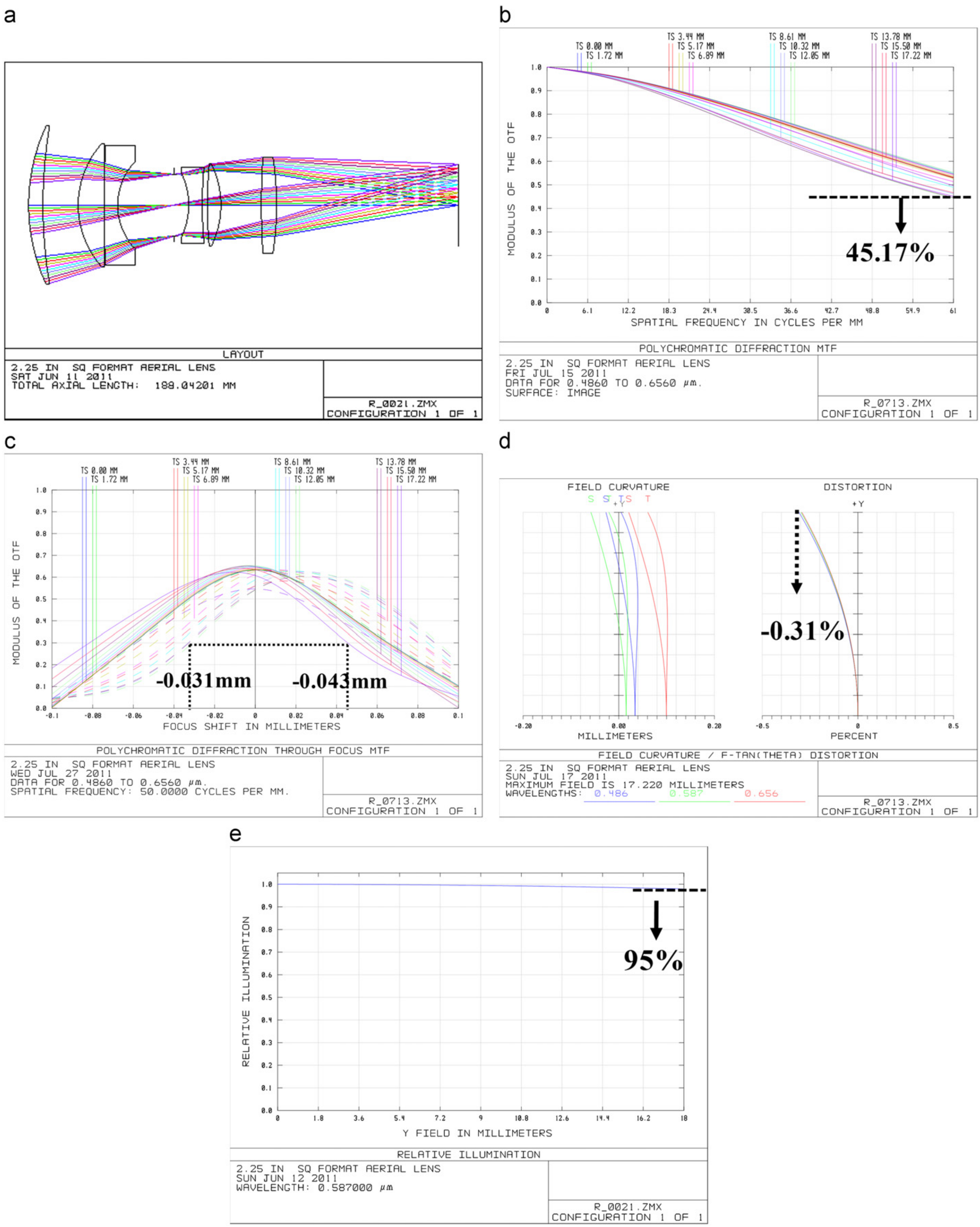

Fig. 7. Image quality of the lens: (a) lens layout after optimization; (b) MTF; (c) through focus MTF; (d) field curvature and distortion; and (e) relative illumination.

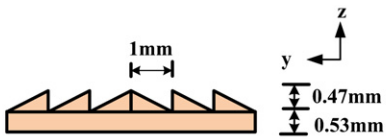

Fig. 8. Specifications for micro-prism arrays.

images, in which the distortion did not exceed $\pm 1\%$. Fig. 7(e) presents the relative illumination which was over 95% in the maximum field of view.

3. Simulation analysis

The micro-prism array was composed of symmetrically rectangular micro-prism arrays. With Eqs. (2) and (3), the base angle of the rectangular prism α was set at 25.1°, the width at 1 mm, and the depth at 0.47 mm, as shown in Fig. 8. Based on the FOV of the lens and the setting distance, the width of the micro-prism array should be at least larger than 76 mm.

3.1. Optical path simulation of micro-prism airborne cameras

Having confirmed the specifications of the lens and the micro-prism arrays, the optical simulation software *LightTools* was applied to the ray tracing simulation for verifying the received optical range of the optical system. First, the micro-prism array was placed 30 mm in front of the optimized lens, the central wavelength λ_G was set 550 nm, and six beams were equipped for the light from different angles. Fig. 9(a) shows the distribution of the simulated ray tracing. The first beam stood for infinite parallel light passing through the upper prism array with the incident angle $\delta_w = 7.21^\circ$ and deflecting on the bottom of the sensor. The second beam stood for infinite parallel light passing through the upper micro-prism with the incident angle $\delta_t = 10.03^\circ$ and imaging on the sensor plane at -7.175 mm. The third beam stood for infinite parallel light passing through the upper micro-prism with the incident angle $\delta_0 = 12.84^\circ$ and imaging on the center of the sensor plane. Contrarily, the fourth, fifth and sixth rays of light stood for infinite parallel light passing through to the lower micro-prism with the incident angles of $\delta_0 = -12.84^\circ$, $\delta_t = -10.03^\circ$, and $\delta_w = -7.21^\circ$ and imaging on the center, at 7.175 mm, and on the top of the sensor plane, respectively (Fig. 9(b)).

Furthermore, having set the inclined angle of the light source of the simulated object as $\pm 10^\circ$ (the light source clockwise heading from the light source normal to *z*-axis was positive; otherwise, it was negative) and placing it on both sides of the received optical range of the lens, the inclined angle of the terrain was actually simulated. The imaging height [13] for the miniature UAV of ServoHeli-40 from ServoHeli was defined 800 m as the imaging distance for this system. The terrain images were then inputted for ray tracing simulation in *LightTools*, where the wavelengths of the light source R, G, B of the objects were set as $\lambda_R = 630$ nm, $\lambda_G = 550$ nm, and $\lambda_B = 470$ nm and the energy $P_R = 0.3554$ W, $P_G = 550$ W, and $P_B = 470$ W, respectively (Fig. 10). Fig. 11 shows the simulated results obtained from the sensor, in which it was proven that an image pair with different viewing angles would be formed when the light source refracted with the micro-prism array.

3.2. Imaging simulation of stereoscopic image pair

The required data for stereoscopic aviation observation and a digital stereoscopic model were received from overlapping

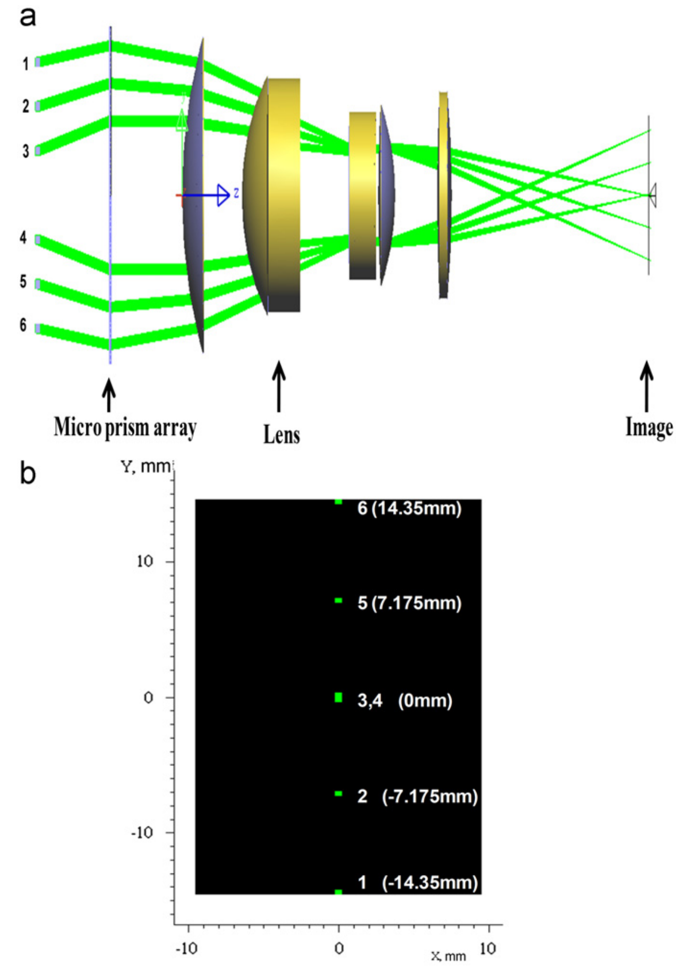

Fig. 9. Infinite optical light passes through prisms: (a) the ray tracing of the system and (b) the position of the received image.

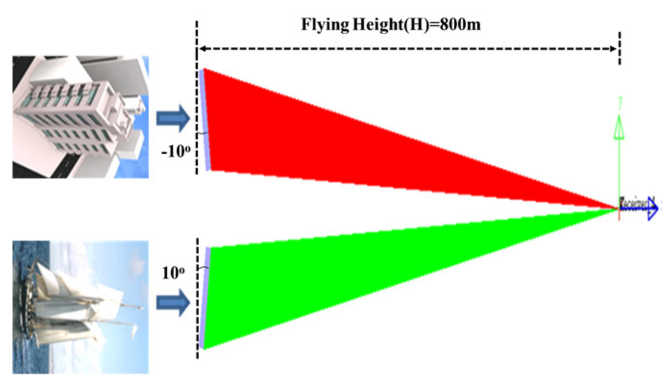

Fig. 10. Simulation of two light sources inclined $\pm 10^\circ$.

stereoscopic image pairs. In this case, the overlapping rate would affect the completeness of the stereoscopic image and the terrain data. This study therefore utilized the geometric relationship between the spectrum-angles of the prism and the aviation height to obtain the distance of the overlapped image pairs, as shown in Fig. 6(b). With Eq. (4) to calculate the distance X from P_1 to P_2, *LightTools* was applied to simulate the imaging of distance X, as shown in Fig. 12(a). When the flying height was $H = 800$ m, the one-shot area was $157.73\ \text{m} \times 111.78\ \text{m}$ and distance X was 283.51 m. The simulated imaging is displayed in Fig. 12(b)

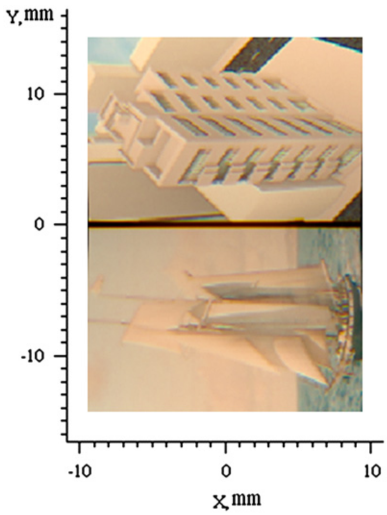

Fig. 11. Simulation of imaging through micro-prism arrays.

and (c):

$$X=(H-T_z)\times(\tan\delta_w+\tan\delta_0)-3T_z\tan\theta_w \quad (4)$$

where H was the flying height, T_z the distance between CCD and the micro-prism array, θ_w the parallel half field of view of the camera, and δ_w and δ_0 the deflection angles after FOV passed through the prism.

From Fig. 12, the images I_{L1} and I_{R2} shot when the aircraft moved from $P_1(x,y,z)$ to $P_2(x',y',z')$ could be formed as a stereoscopic image pair with 100% overlapping rate; but, the errors of the height difference (z-axis) between the two positions and the displacement distance (y-axis) would affect the overlapping rate. In regard to the errors on y-axis and z-axis when the aircraft moving from P_1 to P_2, a stereoscopic image pair with overlapping rate over 95% would be acquired when the imaging distance on y-axis was $X=279.51$ m–287.51 m and the height differences between the two positions $z-z'=-18$ m–18 m, as shown in Fig. 13.

Fig. 14 is the actual stereoscopic image pair with which the terrain model sampled the above designed micro-prism type single-lens 3D aircraft telescope. (Notice that the scale is 1/300, meaning that 1 cm on the map is equal to 300 cm on the real land.) Equal to 800 m height, the terrain image was obtained a left-view and right-view image via micro-prism array as shown in Fig. 14(a) and (b). The red dotted line of both images is the target building. Comparing with both terrain images, there are some different contents, including shadow, relative size, and perspective distortion, in the building because of $\pm 10^\circ$ imaging angle variation. Furthermore, it is further estimated the stereo-images overlapped by the disparity map as shown in Fig. 15. The gray scale indicated the buildings overlap (the dark level shows far distance and the bright level shows near distance) where the overlapping rate of the stereo-image pair was about 100% and the target boundary was integrated. Consequently, the results were successfully verified via this proposed system.

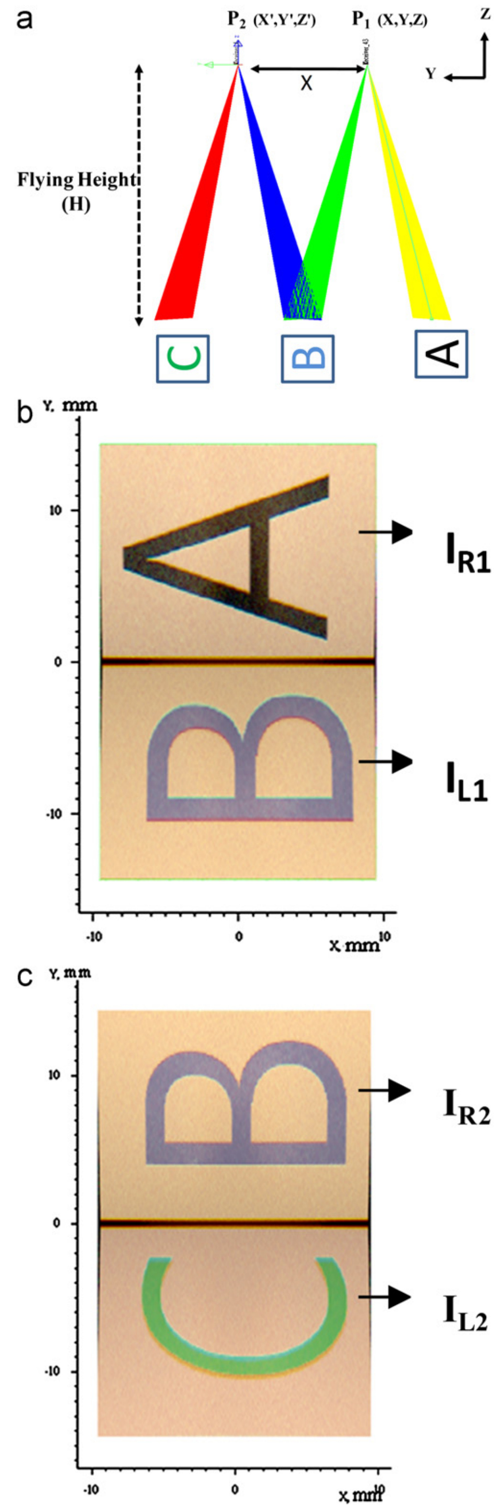

Fig. 12. (a) Setting of optical system from a to b; (b) image shot at P_1; and (c) image shot at P_2.

4. Conclusions

An optical system with a light airborne stereoscopic camera was proposed in this study. The aim was to design a symmetrically rectangular micro-prism array that was 76 mm in length and 1 mm in width, and with a structure that was equipped in front of a remote camera for one-shot-two-view image pairs with an inclined angle ± 10. The optical characteristics of micro-prisms allowed the airborne vertical imaging system to achieve the effects of inclined photography. In comparison with traditional frame type airborne imagers, such a system could acquire highly overlapped stereoscopic image pairs from different viewing angles and the stereoscopic image pairs could be increased by

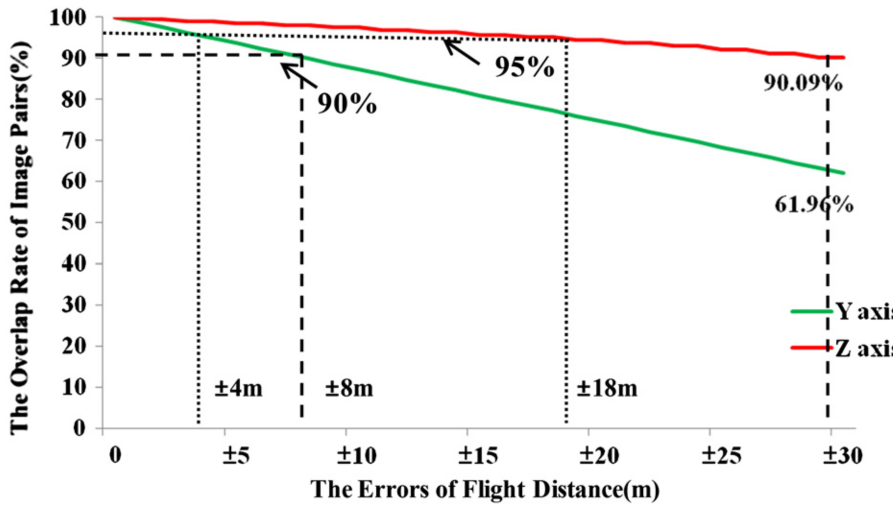

Fig. 13. Relatinship between aviation errors and overlapping rate of images.

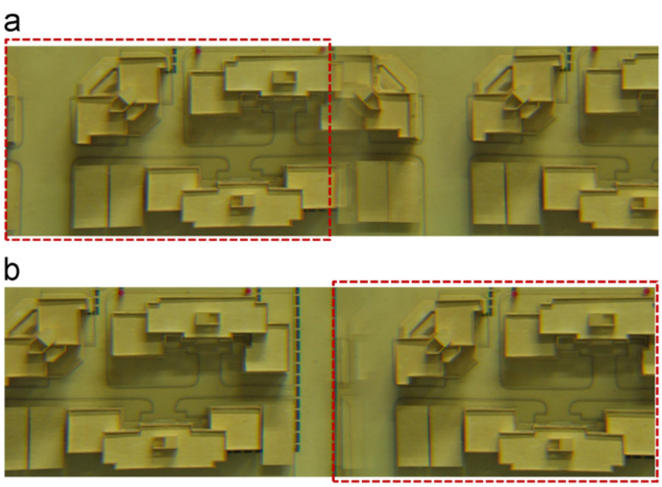

Fig. 14. The terrain samping image of (a) left-viewing and (b) right-viewing.

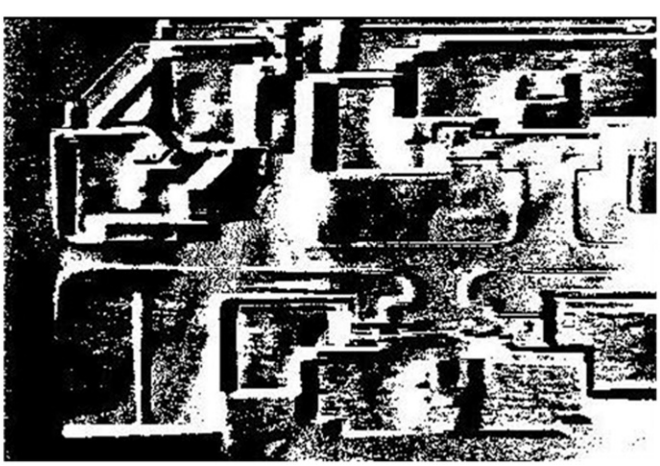

Fig. 15. Disparity map of stereo-image pair.

two-fold. Finally, the optical simulation software, *LightTools*, proved the feasibility of the system imaging the terrain from the height of 800 m, and from the experiments, the terrain sampling image was successfully obtained via the micro-prism type single-lens 3D aircraft telescope. It verified that the micro-prism array could achieve the requirements of inclined imaging and receiving images from two different angles of view.

Acknowledgments

This work is supported by the National Science Council of Taiwan under Contract no. NSC 99-2221-E-224-036 and no. NSC 100-2221-E-224-044.

References

[1] W. Dietrich, C. Wilson, D. Montgomery, J. McKean, Journal of Geology 101 (2) (1993) 259.
[2] M. Jensen, M. Baumann, Y.Q. Chen, IGARSS IEEE International 5 (2008) 7.
[3] E. Frew, T. McGee, Z. Kim, X. Xiao, S. Jackson, M. Morimoto, S. Rathinam, J. Padial, R. Sengupta, Aerospace Conference 5 (2004) 3006.
[4] T. Chen, R. Shibasaki, S. Murai, Photogrammetric Engineering and Remote Sensing 69 (1) (2003) 71.
[5] L. Wang, W.P. Sousa, P. Gong, G.S. Biging, Remote Sensing of Environment 91 (2004) 432.
[6] M. Bader, C.B. Wagoner, Applied Optics 9 (2) (1970) 265.
[7] T.P. Pachidis, John N. Lygouras, Journal of Intelligent and Robotic Systems 42 (2005) 135.
[8] Y. Xiao, K.B. Lim, Journal of Image and Vision Computing 25 (2007) 11.
[9] D.H. Lee, I.S. Kweon, IEEE Transactions on Robotics Automatation 16 (2000) 5.
[10] Y. Chen, T.T. Yang, W.S. Sun, Optics Express 16 (20) (2008) 15495.
[11] 〈http://imaging.nikon.com/lineup/dslr/d3x/spec.htm〉.
[12] M. Laikin, Lens Design, second ed., Marcel Dekker, 1995, 30 pp.
[13] Da-Lei Song, Jun-Tong Qi, Jian-Da Han, Yue-Chao Wang, Acta Automatica Sinica 37 (4) (2011) 480.